SCIENCE CHINA
Information Sciences

June 2023, Vol. 66 160409:1–160409:8
https://doi.org/10.1007/s11432-023-3764-7

• RESEARCH PAPER •
Special Topic: Two-Dimensional Materials and Device Applications

Bolstering functionality in multilayer and bilayer WS_2 via focused laser micro-engraving

Si Min CHAN[1], Eng Tuan POH[1], Jin Feng LEONG[1], Kuan Eng Johnson GOH[1,2,3*] & Chorng Haur SOW[1*]

[1]*Department of Physics, National University of Singapore, Singapore* 117551*, Singapore;*
[2]*Institute of Materials Research and Engineering, Agency for Science, Technology and Research (A*STAR), Singapore* 138634*, Singapore;*
[3]*Division of Physics and Applied Physics, School of Physical and Mathematical Sciences, Nanyang Technological University, Singapore* 639798*, Singapore*

Received 7 March 2023/Revised 28 April 2023/Accepted 9 May 2023/Published online 17 May 2023

Abstract Laser thinning of multilayer transition metal dichalcogenide (TMD) crystals has long been explored for its potential to produce localized domains of optically functional monolayers. Despite the high spatial control and resolution of the laser, the range of appropriate applications for these laser-thinned domains is still limited by the peripheral regions of unaltered thick multilayers. Herein, we report a newfound property of the laser-thinned regions to adhere strongly to the underlying substrate when lasered down to the monolayer limit. Upon a brief sonication in various solvents, the surrounding pristine multilayers can be lifted off, solely leaving behind the post-lasered monolayer patterns. Coupled with the flexible maneuver of the laser, various monolayer designs can be achieved, including micro-antenna, waveguide, and electrode geometries with lateral line widths at 1.5 μm resolution. Furthermore, we also detail the optical properties of the monolayers obtained from laser thinning, with those acquired from multilayers containing more defect-bound excitons, whereas those lasered from bilayers presenting a trion-dominated profile similar to as-grown monolayers. Together, these findings allow for faster and more efficient multilayer removal and areal shaping of optically active monolayer domains, in comparison to multistep and complex standard lithographic etching (lithography–etch–develop) procedures.

Keywords WS_2 monolayer micro-patterning, focused laser, sonication lift-off

Citation Chan S M, Poh E T, Leong J F, et al. Bolstering functionality in multilayer and bilayer WS_2 via focused laser micro-engraving. Sci China Inf Sci, 2023, 66(6): 160409, https://doi.org/10.1007/s11432-023-3764-7

1 Introduction

An ensemble of single crystals with varying layer thicknesses is commonly acquired from typical chemical vapor depositions (CVD) of 2D transition metal dichalcogenides (TMDs). Bilayer and multilayer TMDs are commonly present as by-products of the growth process, in co-existence with the desired monolayer single crystals. Owing to the direct band emission at the monolayer limit [1, 2], extensive research has been dedicated to monolayer TMDs only, exploring its potential for ultrathin optoelectronics [3, 4]. To make multilayer crystals equally functional and reduce material wastage, conscientious efforts have been invested to convert them into monolayers through the use of laser modifications [5–8]. The on-demand generation of these laser-thinned monolayers offers advantageous control over the shape and size of these monolayer domains, yielding tailored nanostructures on the scale of microns or larger. In contrast to conventional mechanical [9–11] and chemical exfoliation [12–14] techniques, the laser thinning process provides enhanced control in monolayer dimensions, while avoiding any unwanted solvent or adhesive residues.

Despite the various advantages associated with the laser thinning process, the applications for these laser-thinned monolayers have generally been restricted to fluorescent micropatterns [15] and simpler

* Corresponding author (email: kejgoh@yahoo.com, physowch@nus.edu.sg)

electronics of regular geometries. While it seems unambiguous that the flexible maneuver of localized laser thinning is suitable for a broad range of customized fluorescent features, the operations to process the monolayers for electronic devices are more complex. With the surrounding multilayer domains alongside the laser-thinned monolayer, the abrupt change in the topographical height profile is expected to cause complications during lithography processes. These height differences, typically hundreds to thousands of nanometres, are larger than the thickness of the evaporated electrodes (tens of nanometres) and can result in electrode damage or asymmetry that would be detrimental to device performance. As such, the laser thinning process usually requires a scan area more extensive than required of the device's active channel to clear out the vicinal multilayers, resulting in prolonged processing time. Comparatively, the alternative to revert to standard lithographic etching procedures would also require additional effort and time to remove the unwanted multilayer domains.

Herein, using a focused laser beam, we transform multilayer and bilayer WS_2 crystals into fluorescence monolayer domains with improved adhesion to the underlying substrate. With the enhanced adhesion, the laser-thinned domains can be exclusively retained when the surrounding pristine multilayers are washed off through a simple sonication in various solvents. This anchoring effect permits a quick and efficient removal of the unwanted peripheral multilayer domains, yielding highly functional WS_2 monolayers of various complex geometries. As such, we demonstrate the capability to craft designed monolayer geometries that are potentially useful for micro-antennas, parallel waveguides, interdigitated supercapacitor electrodes, and hall bar devices. Furthermore, with low temperature measurements, we also reveal valuable insights into the acquired optical properties of the laser-thinned domains, highlighting distinct differences between that obtained from a laser-thinned multilayer and a laser-thinned bilayer. Together, these results support the improvements in operational control to convert as-grown WS_2 multilayers into monolayers of defined geometries and fluorescence profiles for a broader range of applications.

2 Experimental section

WS_2 microflakes are produced via CVD involving two different recipes. For the first method, the seeding promoter, perylene-3,4,9,10-tetracarboxylic acid tetrapotassium salt (PTAS) is added to the substrate to promote the growth of the microflakes. Si/SiO_2 substrates are first rinsed with acetone, isopropanol, and distilled water. A few drops of the PTAS solution are drop-casted at the center of the substrate. The precursors used for the reaction are tungsten oxide (WO_3) and sulfur (S) powders purchased from Sigma Aldrich. Together with the PTAS-treated substrate, WO_3 powder is placed at the point of the furnace with the highest temperature. Sulfur powder is placed at the upstream of the furnace with a temperature of approximately 200°C. The furnace is first maintained at 25°C with 50 sccm argon flow for 140 min to purge the chamber. Then, with the same gas flow, the furnace is ramped up to 780°C at a rate of 25°C/min and maintained at the highest temperature for 6 min. Lastly, the furnace is left to cool down naturally to room temperature.

The second method involves the same arrangement as the above method with a few changes. Instead of the seeding promoter, a mixture of sodium chloride (NaCl) and tungsten oxide ($WO_{2.9}$) in a 1:5 ratio is used as the metal precursor to promote the growth of microflakes by reducing the melting point of the precursor. The use of this recipe eliminates any possibility that the selective anchoring effect could be due to the treated substrate. In this study, it has been shown that there is no distinction in the effect of selective anchoring between the microflakes grown using the two different recipes. The furnace is first maintained at 25°C with a flow of argon gas at 80 sccm for 140 min to purge the chamber. Under the same gas flow, the furnace is then ramped up to 800°C at a rate of 25°C/min and maintained at the highest temperature for 9 min. Lastly, the furnace is left to cool down to room temperature naturally.

Large area MoS_2 multilayer sheets are grown using a similar CVD setup with different chemical precursors. Typically, a portion of molybdenum chloride ($MoCl_5$) is placed at the center of the furnace with the highest temperature, while the sulfur (S) powder is emplaced further upstream. Receiving substrates comprising strips of 300 nm SiO_2 on Si are placed a few centimeters downstream from the molybdenum precursor. Subsequently, the furnace is heated to 850°C (with sulfur temperature at 300°C) at a rate of 28°C/min, with constant argon flow of 50 sccm under a pressure of 2 Torr. The system is held at the highest temperature for 10 min, before it is cooled naturally to room temperature. The layer number of the thin films is controlled by either the amount of $MoCl_5$ precursors used or the total pressure in the system.

The focused laser beam setup comprises an upright optical microscope with a side port that allows a parallel laser beam to enter. Once inside the optical microscope, the laser beam is reflected toward the objective lens by a beam splitter. A diode pump solid-state laser (Sintec VD-IIA DPSS Laser Driver) emitting laser light at a wavelength of 532 nm is utilized. An objective lens with a magnification of 100× is employed, giving rise to a focused laser spot of ∼3 μm^2. The sample is placed on a motorized sample stage. In this work, we fix the position of the focused laser beam while the sample is moved across using a motorized sample stage. With the programmed stage connected to a computer, laser patterning can be carried out with step size in the μm range. Laser power is varied between 20 to 70 mW, while scanning velocity is typically at 15 μm/s for rastering and 100 μm/s for controlled patterning of any designed microstructure. The entire laser modification process is captured by a charged-coupled device (CCD) camera, allowing examination of the sample and process in real-time. Characterization of the sample is carried out through optical and fluorescence microscopy (Olympus BX51), scanning electron microscopy (JEOL-JSM 6440F), and photoluminescence (PL) spectroscopy (Witec Laser 532 nm).

3 Results and discussion

Figure 1(a) presents a schematic overview of the focused laser setup utilized in this work. The laser beam is directed into a microscope and focused through the objective lens upon the sample emplaced on a computer-linked microcontroller stage, allowing for real-time view of the laser-modification process. The flexibility of the laser setup permits laser-thinned patterns with micrometer resolution and reproducibility across a broad range of laser powers. Figures 1(b) and (c) show the optical (OM) and fluorescence (FM) micrographs of a WS_2 multilayer engineered with a spiral micropattern in the interior region. Under the influence of the laser, the multilayer is thinned down to monolayer thickness, with optical contrast similar to the peripheral monolayer domains of the microflake. More importantly, the modified spiral exhibits distinct fluorescence, reiterating the laser thinning process and the potential of the technique for micropatterning applications. The laser-sculpting process is trialed upon WS_2 bilayers as well, with similar OM and FM displays presented under Figures 1(d) and (e). Despite a similar range of laser power incident upon the thinner bilayer (as compared to thicker multilayers), the laser thinning process is found to be self-limiting at the monolayer limit, as evidenced by the discernible emission from the intersecting line cuts in Figure 1(e). Upon laser treatment, the modified domains are endowed with enhanced adhesion onto the underlying SiO_2 substrate. Figure 1(f) presents an OM image of a WS_2 microflake that is laser-thinned across the lower half by laser raster. After mild sonication amidst isopropanol solvent, the unaltered multilayer domain of the sample is lifted off, leaving behind the laser-modified region firmly anchored onto the substrate (Figure 1(g)). Herein, it is imperative to note that any CVD grown pristine WS_2 monolayers present on the substrate were also lifted off during the solvent step; the monolayer regions acquired from laser modification display stronger substrate adhesion when benchmarked against CVD grown monolayer triangles.

To provide greater insight into the nature of the fluorescence emission, the dominant exciton species contributing to the fluorescence from the laser-treated multilayer WS_2 are identified under low temperature (77 K) PL spectroscopy. Figure 2(a) presents a multilayer WS_2 crystal laser-thinned through a raster over the top half of the sample, with the corresponding fluorescence distribution in Figure 2(b). Unsurprisingly, the laser-modified region exudes a uniform red contrast against the altered regions. From a single spot (red "x" marked in Figures 2(a) and (b)) measurement, the acquired low temperature PL is displayed in Figure 2(c). Deconvoluted into the separate discrete peaks, the subsequent peak fit assignments for the spectrum ascertain the dominant contribution of defect-bound excitons from the emission of the laser-thinned multilayer. As the laser ablates through the multiple upper layers of the WS_2 crystal, the inconsistent extents of laser-induced sublimation [6] for the various layers would invariantly result in uneven laser influence across the surface of the bottommost monolayer, generating a multitude of dangling bonds and chalcogen vacancies. Comparatively, the low temperature PL profile of a CVD as-grown WS_2 monolayer (Figure 2(d)) comprises mainly trion-based emissions due to its inherent n-type nature stemming from the high density of sulfur vacancies (V_O) [16,17]. Under Raman investigation (Figure 2(e)), a comparative study of the lasered region against the pristine revealed a substantial decline in the magnitude for both in-plane E^1_{2g} and out-of-plane A_{1g} signals, assuring the successful layer reduction process without obvious precipitation of any side product WO_x signals.

Despite apparent similarities in optical contrast and fluorescence for the laser thinning process of mul-

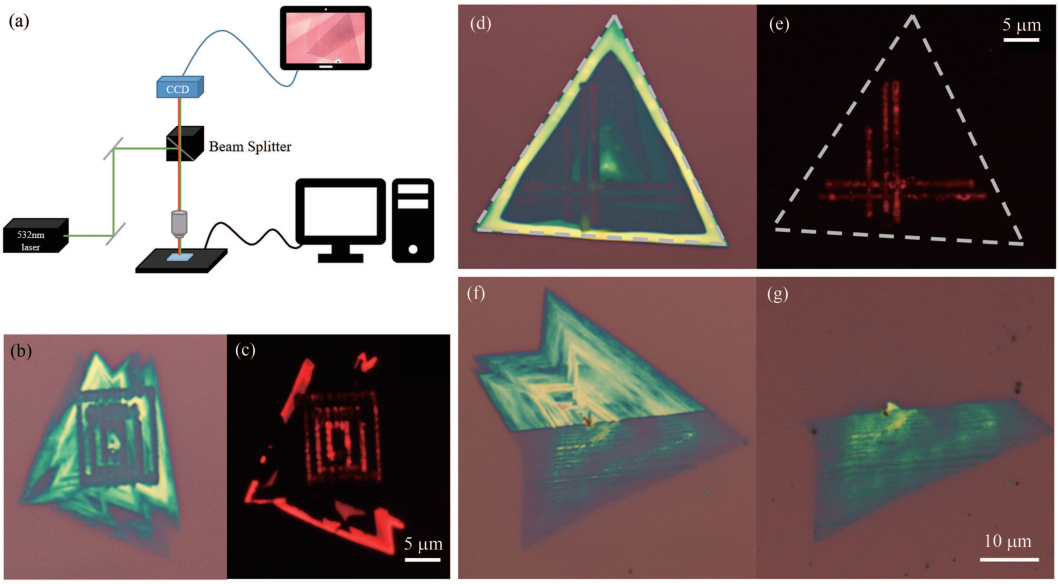

Figure 1 (Color online) Summary of laser processed outcomes for various multilayer WS_2 crystals. (a) Schematic illustration of the focused laser beam setup. (b) OM image of a multilayer WS_2 microflake with a laser-engineered micropattern within. (c) Corresponding FM image of the patterned microflake in (b). (d) OM image of a bilayer WS_2 microflake laser-thinned with intersecting lines. (e) Corresponding FM image of the patterned bilayer in (d). (f) OM image of a WS_2 multilayer laser-thinned across half the crystal domain through laser sweep raster (g) OM of the laser-treated microflake in (f) after washing in isopropanol. The lasered region remains firmly anchored onto the substrate while the pristine multilayer region is washed off.

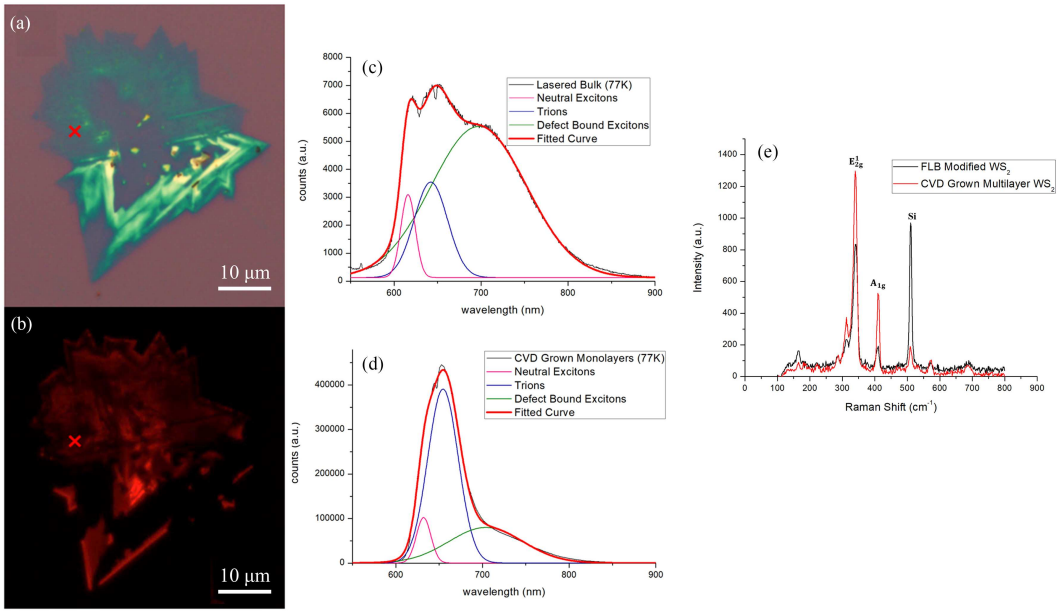

Figure 2 (Color online) Optical characterization of laser-thinned domains of multilayer WS_2. (a) OM image of multilayer WS_2 laser-modified across the top-half domain of the crystal. (b) Corresponding FM image of laser-modified multilayer WS_2 in (a), demonstrating the uniform fluorescence from the laser-thinned top-half domain. (c) Low temperature PL characterization (77 K) acquired from the single spot red "x" marked out in (a) and (b). The various peak components deconvoluted from the spectrum are fitted in correspondence to the contributions from neutral excitons, trions, biexcitons, and defect-bounded excitons. (d) Low temperature PL characterization (77 K) obtained from an as-grown pristine WS_2 monolayer. Comparison across spectra in (c) and (d) presents distinct contrast in spectra weightage of trions and defect-bound excitons after laser modification. (e) Raman spectra comparison for the pristine multilayer WS_2 against the laser-modified region.

tilayer and bilayer WS_2 micro flakes, flagrant differences are observable in the respective PL profiles. Figure 3(a) introduces bilayer WS_2 crystals typically acquired from the layer ensemble within a single substrate of CVD grown WS_2 crystals. Under the influence of the focused laser beam, the clean-cut patterns engraved within the bilayer sample emit a distinct red fluorescence with greater intensity (Figure 3(b))

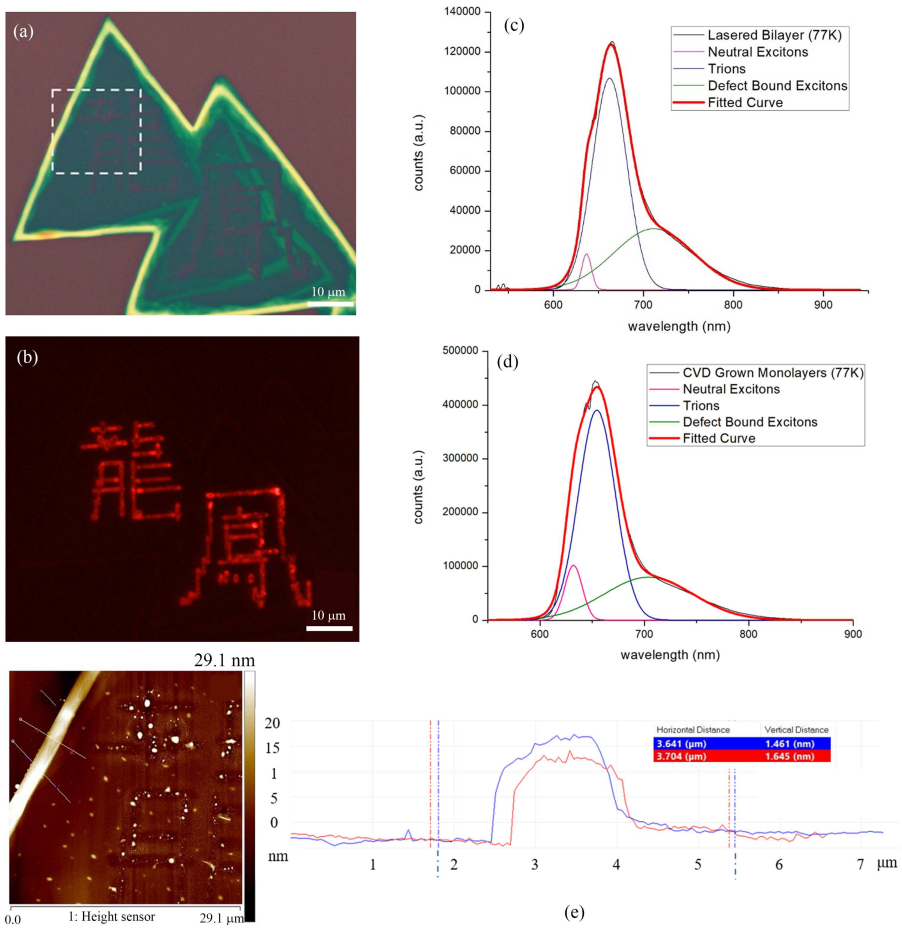

Figure 3 (Color online) Optical characterization of laser-thinned domains of bilayer WS_2. (a) OM image of a bilayer WS_2 crystal after laser-modification within the center domain of the crystals. (b) Corresponding FM image of laser-modified bilayer WS_2 in (a), demonstrating a clear fluorescence outline of the laser-carved characters in the laser-thinned domain. (c) Low temperature PL characterization (77 K) acquired from a single spot domain amidst the fluorescent active laser-carved characters in (b). The various peak components deconvoluted from the spectrum are fitted in correspondence to the contributions from neutral excitons, trions, biexcitons, and defect-bounded excitons. (d) Low temperature PL characterization (77 K) obtained from an as-grown pristine WS_2 monolayer. Comparison across spectra in (c) and (d) presents minor alterations in the spectra weightage of the various exciton species after laser modification. (e) AFM characterization of the bilayer sample edge near the laser-engraved pattern, demonstrating height thickness of approximately 1.5 nm in assurance of the bilayer identity.

as compared to that obtained from lasered multilayers (Figure 2(b)). In comparison to the imperfect thinning of multilayers due to inconsistent laser penetration across the multiple overlying layers, the laser thinning of bilayers is likely to provide a cleaner ablation of the top layer at greater uniformity and retain a higher quality surface of the underlying monolayer. The resultant emission is mainly contributed by trions (Figure 3(c)), with low temperature peak profile analogous to a CVD as-grown monolayer crystal (Figure 3(d)). Herein, it is imperative to note that the difference in emission profile and monolayer quality between laser-thinned multilayers and bilayers offers flexibility in utilizing these samples for different applications. The high-quality, trion-dominated lasered bilayer would serve useful in replacement of as-grown monolayers for optoelectronic studies, while the defect-dominated lasered multilayer would apply for studies involving defect-related quantum emitters. Under scrutiny of the atomic force microscopy (AFM) instrumentation, the bilayer nature of the sample is further ascertained by the height difference between the sample and substrate in the range of 1.45–1.65 nm (Figure 3(e)).

To further develop the capability of the focused laser micro-engraving technique, the effect of solvent sonication is investigated for selective wash-off at specific sample domains. Upon brief sonication of the laser-modified multilayer samples in the various solvents (acetone, isopropanol, and water), the laser-thinned monolayer domains are retained, while the surrounding multilayers are efficiently removed. Remarkably, the laser thinning process provides an additional mechanical influence at anchoring the lasered domain with greater adhesion to the underlying substrate, which we postulate to arise from

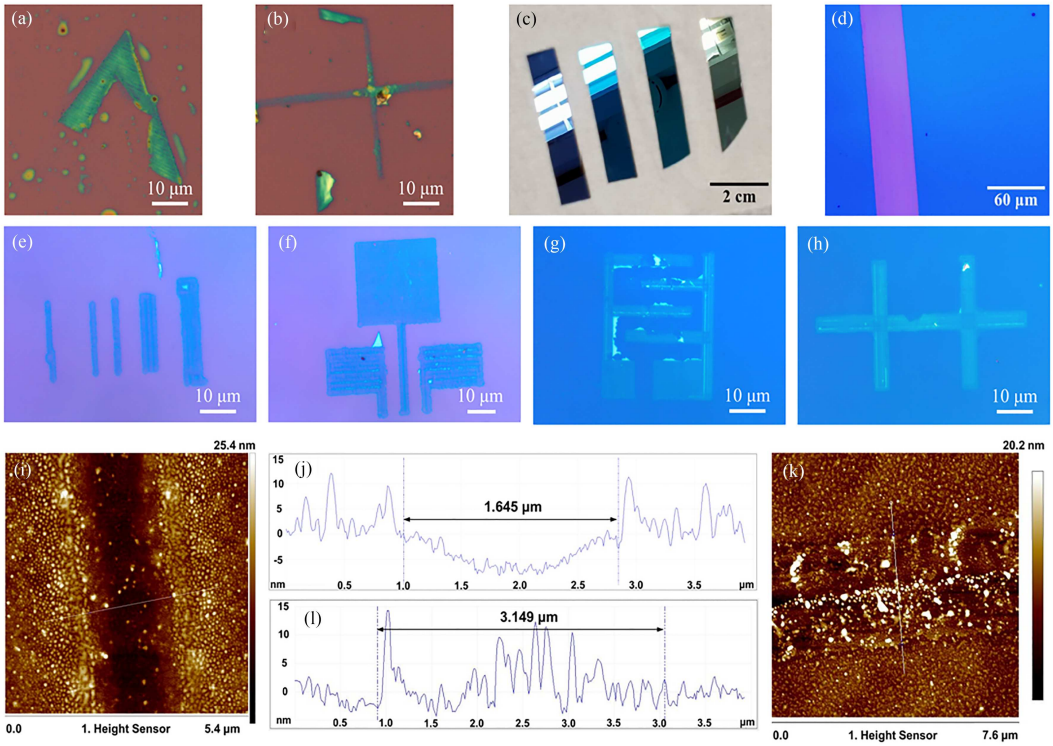

Figure 4 (Color online) Selective solvent wash-off of pristine multilayer domains for complex device geometry designs. (a) OM image of remnant irregular laser-thinned domain of WS_2 multilayer after brief sonication in acetone. (b) OM image of remnant laser-thinned cross structure of WS_2 multilayer after brief sonication in isopropanol. (c) OM image displaying the sample strips of MoS_2 thin film with varying thicknesses obtained from CVD growth. (d) Zoomed in OM of thin film domain from a single sample of multilayer MoS_2 thin film. The sample is intentionally scratched to demonstrate the presence of the uniform thin film. (e) Parallel array comprising monolayer waveguide bars of varying dimensions obtained from post-laser-thinning wash of the sample in deionized water. (f) Laser-thinned monolayer of micro antenna device geometry obtained from post-laser washing of the sample in deionized water. (g) Monolayer domain of interdigitated micro-capacitor geometry obtained from post-laser washing of the sample in deionized water. (h) Cross hall bar geometric monolayer domain obtained from post-laser anchoring after sonication in deionized water. (i) AFM characterization across the laser-crafted trench due to laser thinning, along with the associated (j) cross-section profile demonstrating the feature width at 1.645 μm. (k) Similar AFM characterization across to-and-fro two-lined laser raster, along with the associated (l) cross-section profile demonstrating the double-lined feature width doubled at 3.149 μm.

radiation pressure accumulated from momentum transfer of the photon ensemble impinging upon the sample. The process is found to be reproducible for various solvents, with impressive patterning flexibility as presented in Figures 4(a) and (b). These OM images prove that the laser-anchor-and-wash process can be utilized for patterns dependent upon the original multilayer geometry (Figure 4(a)) as well as self-designed geometries (crossbar in Figure 4(b)) within the size constraints of the as-grown WS_2 multilayer/bilayer samples. The relatively clean washes for the samples in both acetone (Figure 4(a)) and isopropanol (Figure 4(b)) reassure the ease of the technique to create monolayer-only nanostructures for potential studies in optoelectronics and wave-mixing waveguides respectively.

In order to expand the collection of multilayer samples suitable for laser-carving, and accommodate a broader range of complicated device geometries, multilayer MoS_2 thin films are grown and processed under similar laser conditions. Figure 4(c) displays the CVD grown MoS_2 thin films uniformly coated over the centimeter scale substrates, with sample thicknesses controllable by varying the growth conditions [18]. The high uniformity and quality of the film are further assured through high magnification OM in Figure 4(d), with a scratch-out to prove the presence of the continuous thin film. When subjected to refined laser thinning, followed by light washing in deionized water, a range of defined monolayer patterns are also achieved. This not only reiterates the universality of the technique for different solvents and materials, but also reassures the capability to larger scale production of a diverse range of functional monolayer structures in preparation for various applications. In Figure 4(e), a parallel array of bar structures with different widths and lengths presents opportunity for evanescent sensing waveguides with customizable properties [19, 20]. Figure 4(f) demonstrates a structure of three isolated panels that could serve as a micro-antenna when completed with SMA connections [21], while the interdigitated geometry in

Figure 4(g) would be useful as a high-performance micro-supercapacitor [22–24]. In contrast, a simpler crossbar geometry as shown in Figure 4(h) could be exploited for hall-bar measurements across the monolayer semiconductor. To evaluate the achievable resolution with this technique, the feature widths were measured across a single-line laser scan and a two-line laser raster using an AFM. As shown in Figures 4(i) and (j), the single line scan profile produced a laser-thinned domain of 1.645 μm in width, in fair consistency with the doubled width of 3.149 μm (∼1.575 μm per line) for the two-line raster in Figures 4(k) and (l). Together, these results reassure the capability of this facile laser-thin and solvent wash method to flexibly engineer a wide variety of clean and well-defined (resolution ∼1.5 μm) structures for a plethora of device applications.

4 Conclusion

In this study, we evaluate the optical and mechanical influence of the focused laser beam upon multilayer and bilayer WS_2 crystals. Across a broad range of laser intensities, the beam causes localized thermal sublimation of the upper layers, leaving behind fluorescence active monolayer domains of different optical properties. With laser-thinned multilayers, defect-dominant monolayer regions can be realized for optical studies involving defect-bound excitonic emissions. In contrast, the lasered thinned bilayers yielded quality monolayers that possess trion-dominated optical profiles that are comparable to as-grown CVD monolayers. This presents an effective engineering tool to design functional monolayers with controllable emission profiles applicable for various relevant studies. Furthermore, with a subsequent sonication step amidst various solvents (acetone, isopropanol, water), the laser's capability to improve sample adhesion at the local laser-thinned regions is revealed. This micro-anchoring process permitted clean retention of the lasered domain while the unaltered peripheral multilayers are liberated off. The same approach is also applicable to MoS_2 thin films. As a result, complicated designs of functional monolayer domains can be crafted without hindrance from any surrounding thick multilayers, allowing the ease of flexibly shaping monolayer crystals for a myriad of applications without the need for complex multistep lithographic processes.

Acknowledgements This work was supported by Agency for Science, Technology and Research (A*STAR) (Grant No. 15270000-16). Kuan Eng Johnson GOH acknowledges support from Agency for Science, Technology and Research (Grant No. #21709) and Singapore National Research Foundation (Grant No. CRP21-2018-0001).

References

1 Mak K F, Lee C, Hone J, et al. Atomically thin MoS_2: a new direct-gap semiconductor. Phys Rev Lett, 2010, 105: 136805
2 Splendiani A, Sun L, Zhang Y, et al. Emerging photoluminescence in monolayer MoS_2. Nano Lett, 2010, 10: 1271–1275
3 Mak K F, Shan J. Photonics and optoelectronics of 2D semiconductor transition metal dichalcogenides. Nat Photon, 2016, 10: 216–226
4 Lopez-Sanchez O, Lembke D, Kayci M, et al. Ultrasensitive photodetectors based on monolayer MoS_2. Nat Nanotech, 2013, 8: 497–501
5 Gong L, Zhang Q, Wang L, et al. Emergence of photoluminescence on bulk MoS_2 by laser thinning and gold particle decoration. Nano Res, 2018, 11: 4574–4586
6 Castellanos-Gomez A, Barkelid M, Goossens A M, et al. Laser-thinning of MoS_2: on demand generation of a single-layer semiconductor. Nano Lett, 2012, 12: 3187–3192
7 Lu J, Lu J H, Liu H, et al. Improved photoelectrical properties of MoS_2 films after laser micromachining. ACS Nano, 2014, 8: 6334–6343
8 Akkanen S M, Fernandez H A, Sun Z. Optical modification of 2D materials: methods and applications. Adv Mater, 2022, 34: 2110152
9 Liu N, Kim P, Kim J H, et al. Large-area atomically thin MoS_2 nanosheets prepared using electrochemical exfoliation. ACS Nano, 2014, 8: 6902–6910
10 Magda G Z, Pető J, Dobrik G, et al. Exfoliation of large-area transition metal chalcogenide single layers. Sci Rep, 2015, 5: 14714
11 Li H, Wu J, Yin Z, et al. Preparation and applications of mechanically exfoliated single-layer and multilayer MoS_2 and WSe_2 nanosheets. Acc Chem Res, 2014, 47: 1067–1075
12 Eda G, Yamaguchi H, Voiry D, et al. Photoluminescence from chemically exfoliated MoS_2. Nano Lett, 2011, 11: 5111–5116
13 Zeng Z, Yin Z, Huang X, et al. Single-layer semiconducting nanosheets: high-yield preparation and device fabrication. Angew Chem Int Ed, 2011, 50: 11093–11097
14 Nicolosi V, Chhowalla M, Kanatzidis M G, et al. Liquid exfoliation of layered materials. Science, 2013, 340:
15 Venkatakrishnan A, Chua H, Tan P, et al. Microsteganography on WS_2 monolayers tailored by direct laser painting. ACS Nano, 2017, 11: 713–720

16 Gutiérrez H R, Perea-López N, Elías A L, et al. Extraordinary room-temperature photoluminescence in triangular WS_2 monolayers. Nano Lett, 2013, 13: 3447–3454
17 Cong C, Shang J, Wu X, et al. Synthesis and optical properties of large-area single-crystalline 2D semiconductor WS_2 monolayer from chemical vapor deposition. Adv Opt Mater, 2014, 2: 131–136
18 Yu Y, Li C, Liu Y, et al. Controlled scalable synthesis of uniform, high-quality monolayer and few-layer MoS_2 films. Sci Rep, 2013, 3: 1866
19 Block A, Etrich C, Limboeck T, et al. Bloch oscillations in plasmonic waveguide arrays. Nat Commun, 2014, 5: 3843
20 Yang Y, Guo Y, Huang Y, et al. Crosstalk reduction of integrated optical waveguides with nonuniform subwavelength silicon strips. Sci Rep, 2020, 10: 4491
21 Naji D K. Design of compact dual-band and tri-band microstrip patch antennas. Int J Electromagn Appl, 2018, 8: 26–34
22 Ray A, Roth J, Saruhan B. Laser-induced interdigital structured graphene electrodes based flexible micro-supercapacitor for efficient peak energy storage. Molecules, 2022, 27: 329
23 Cao L, Yang S, Gao W, et al. Direct laser-patterned micro-supercapacitors from paintable MoS_2 films. Small, 2013, 9: 2905–2910
24 Xiao Y, Huang L, Zhang Q, et al. Gravure printing of hybrid MoS_2 @S-rGO interdigitated electrodes for flexible microsupercapacitors. Appl Phys Lett, 2015, 107: 013906